Inlet Dynamics and Compressor Surge

RONALD A. MAYS*
The Boeing Company, Seattle, Wash.

A numerical solution of the one-dimensional, unsteady, inviscid flow equations in a variable area duct, based on Lax's artificial viscosity technique, was developed to examine large amplitude transients, such as compressor surge, and their effect on mixed-compression inlet flow. The advantages and characteristics of the numerical method are briefly outlined. How to properly define surge, the appropriate numerical boundary conditions, and the sensitivity of inlet flow history to the surge-initiating mechanism are discussed. Representative experimental data are evaluated and compared with numerical results.

Nomenclature

A = flow area
a = sound speed
k = dissipative coefficient
M = Mach number
P = pressure
T = temperature
t = time
u = velocity
x = spatial coordinate
γ = specific heat ratio
ρ = density
ψ = bleed flow

Superscripts

n = temporal index
0 = initial condition

Subscripts

C = cowl
H = hammer wave
ℓ = spatial index
o = nondimensionalized form
r = reference condition
T = total conditions
TH = throat

Introduction

THE analytical study of large-scale transient flow phenomena in supersonic inlets and their interaction with the engine flow is of primary importance to the inlet designer. The optimum design of the inlet, its associated auxiliary air systems, and the inlet control system in part hinge on an understanding of the effect of these transients on the inlet flow history and their attendant effect on inlet control and performance. A representative axisymmetric, mixed-compression inlet configuration is shown in Fig. 1. The variable flow geometry is provided by axially translating the centerbody and modulating the throat doors. The indicated auxiliary air systems perform a variety of functions. Boundary-layer bleed reduces the boundary-layer thickness, thus providing some measure of shock stability and improving the compressor face pressure recovery. The aerodynamically actuated throat slot bleed stabilizes the normal shock by restricting its upstream travel when the inlet is subjected to small, rapid freestream and engine transients. The bypass system spills the air not required by the engine or other systems during off-design operation, maintains the terminal normal shock at the desired supercritical position by sensing changes in the throat total pressure and subsonic diffuser static pressures, and provides additional engine air during takeoff. The secondary air system provides cooling air for the exhaust nozzle and the cabin air-conditioning system, and acts as an internal bypass duct to alleviate inlet-engine mismatch.

Past inlet dynamics studies have relied mainly on the linearized small perturbation method,[1] the lumped mass method,[2,3] or the more complex method of characteristics.[4,5,6] The "small perturbation" method assumes that the dependent variables deviate only slightly from their steady-state values. By neglecting higher-order terms, the differential equations can be linearized and solved handily. While such a flow description is satisfactory for the study of acoustic phenomena, for example, the range of inputs that can be adequately described by this linear technique is somewhat restricted. The "lumped mass" method is a quasi-steady-state scheme which assigns average flow properties throughout the inlet, introduces mass bleed and viscous effects as added empirical correction factors and approximates transient flow phenomena by using transfer functions to simulate pressure signal transit times. The "method of characteristics" is, of course, the most rigorous technique. The governing differential equations are rewritten in a form that allows the flow parameters ρ, u, and P to be calculated iteratively along characteristic lines in the x-t plane. However, the existence or the formation of shock waves, either as a result of the initial field prescription or the rapid variation in the boundary conditions, appreciably complicates the programming requirements of this implicit finite difference method by dividing the flowfield into distinct flow regions at whose boundaries the flow properties are discontinuous.

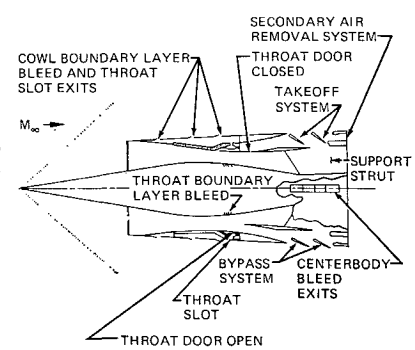

Fig. 1 Axisymmetric mixed-compression inlet.

Presented as Paper 69-484 at the AIAA 5th Propulsion Joint Specialist Conference, U.S. Air Force Academy, Col., June 9–15, 1969; submitted June 19, 1969; revision received January 5, 1970. The author would like to thank J. D. Craig for writing the computer program and K. E. Mills and W. D. Henckel for performing many of the numerical experiments.

* Senior Engineer, Propulsion Research Unit, Commercial Airplane Group. Associate Member AIAA.

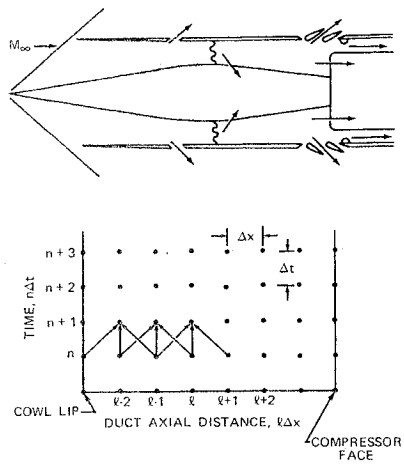

Fig. 2 Inlet schematic and calculation grid.

The availability of larger, faster computing machines now allows the complete governing nonlinear equations (conservation of mass, momentum, and energy) to be solved by conceptually simple and more generally applicable explicit finite difference methods. These techniques circumvent many of the difficulties inherent in the other schemes by dealing with modified forms of the governing differential equations directly. The time and spatial derivatives in the differential equations are represented by the sums and differences of truncated Taylor's series expansions about the point where the derivatives are being evaluated. Using Lax's[7] method, solving partial differential equations is thereby reduced to solving explicit algebraic equations.

The large inlet flow fluctuations that accompany compressor surge may structurally damage the inlet and its auxiliary systems. The postulated causes of such surges are many and varied and include atmospheric turbulence, localized changes in inlet angle of attack, acoustical resonance, mechanical failures in the fuel control or exhaust nozzle systems, and even human errors in system maintenance. Unless such anomalies are considered in the system design, the resulting inlet structural failure could have a serious effect on the airplane stability and control. Therefore, a study was undertaken to examine the nature of these surges and their concomitant effects on the inlet flow history. How does one properly define compressor surge? To what extent does this definition influence the resulting inlet flow history? How dependent is this definition on the inlet-engine combination? How do the inlet geometry and auxiliary air systems affect or modify the flow following such a surge? It is to these questions that we address ourselves.

Method

Past difficulties in solving the inviscid, unsteady equations for a perfect gas by the finite difference method have centered around the discontinuous nature of the solutions to these equations. These solutions are characterized by continuous flow regions separated by discontinuities such as shock waves or contact surfaces. Treating the complete equations in any conventional manner, such as the method of characteristics, results in a highly implicit set of coupled equations that must be solved iteratively. The programing required for such schemes is considerable, but unavoidable.

To hurdle these substantial obstacles, numerical techniques have been devised that eliminate the discontinuous nature of the governing equations by effectively adding dissipative terms to the equations, thereby replacing the troublesome discontinuities by continuous flow regions. These added nonphysical terms can be made sufficiently small to limit their effect to these formerly discontinuous regions. The Rankine-Hugoniot equations are satisfied across these artificially continuous shock waves and the wave thickness can be made negligibly small by a suitable choice of grid dimensions. The particular method used here was developed by Lax.

The governing differential equations are

mass,

$$\partial(\rho A)/\partial t + \partial(\rho A u)/\partial x + \psi = 0$$

momentum,

$$\partial(\rho A u)/\partial t + \partial(\rho A u^2)/\partial x + \psi u = -A(\partial P/\partial x) \quad (1)$$

and energy,

$$\partial\{(\rho A)[P/(\gamma-1)\rho + u^2/2]\}/\partial t + \partial\{(\rho A u)[\gamma P/(\gamma-1)\rho + u^2/2]\}/\partial x + \psi[\gamma P/(\gamma-1)\rho + u^2/2] = 0$$

In these equations, ψ represents the lateral bleed flow from the inlet. Fluid with the mainstream momentum and enthalpy is discharged laterally at a rate determined by the mainstream static pressure, total temperature, a bleed or plenum back pressure, and a lateral bleed area. This is effectively a boundary-layer type of bleed simulation.

The governing differential equations have the general form

$$\partial f/\partial t + \partial g/\partial x + h = 0 \quad (2)$$

where f, g, and h are functions of space and time. For example, in the mass conservation equation, $f = \rho A$, $g = \rho A u$, and $h = \psi$.

The Lax technique replaces the normally used forward time difference by an averaged time difference. Using this and the central spatial difference notation, the general form of the difference equations becomes

$$\{f_l^{n+1} - \tfrac{1}{2}[f_{l+1}^n + f_{l-1}^n]\}/\Delta t + \{g_{l+1}^n - g_{l-1}^n\}/(2\Delta x) + h_l^n = 0 \quad (3)$$

The subscript is the spatial index $x = \ell\Delta x$. The super script is the temporal index $t = n\Delta t$. The inlet schematic and calculation grid are illustrated in Fig. 2. The calculations proceed forward in time as indicated. Given the initial and boundary conditions (ρ_l^n, u_l^n, and P_l^n are known for all ℓ and n), ρ_l^{n+1}, u_l^{n+1}, and P_l^{n+1} can be determined by successively solving the three conservation difference equations. Moving from left to right, the flow variables are calculated explicitly at each spatial node ℓ. Reaching the right-hand boundary, the temporal index is increased (all $n+1$ quantities become n quantities) and calculations begin again at the left-hand boundary.

If one were to use conventional forward time and central spatial differences, the same difference algorithm could be obtained from differential equations of the form

$$\partial f/\partial t + \partial g/\partial x + h = k\cdot\partial^2 f/\partial x^2 \quad (4)$$

where

$$k = (\Delta x)^2/2\Delta t$$

Averaging the time derivatives is therefore equivalent to adding dissipative second-order terms to the differential equations. Dimensionally, k corresponds to a molecular diffusivity coefficient in the mass equation, a kinematic viscosity coefficient in the momentum equation, and a combined kinematic viscosity and thermal diffusivity coefficient in the energy equation. However, the magnitude of k is necessarily several orders of magnitude larger than any physical counterpart, and some care must be taken in interpreting the numerical data to ensure that no physical significance is attached to results that are really attributable to the localized effect of these second-order terms. Given suitable initial and boundary conditions, the difference equations are explicit in time. No iteration or special equations

are required to handle the shock waves present initially or generated at the boundaries.

The degree to which the numerical solution departs from the inviscid solution depends on the magnitude of the coefficient k. This relation can be seen more clearly if the dissipative differential equations are nondimensionalized. We begin by defining the following dimensionless ratios

$$u_o = u/u_r,\ P_o = P/\rho_r u_r^2$$
$$\rho_o = \rho/\rho_r,\ x_o = x/x_r,\ t_o = t/(x_r/u_r) \tag{5}$$

The subscript r implies a reference quantity and the subscript o implies a dimensionless ratio. The reference velocity u_r was chosen to be an average value and will be discussed later, x_r is the inlet length, and ρ_r is the freestream density.

Substituting these dimensionless ratios yields a set of equations in which the only coefficient appearing is the ratio $k/u_r x_r$ in the second-order terms. This coefficient can be rewritten as

$$[(\Delta x/\Delta t)/2u_r]/(x_r/\Delta x) \tag{6}$$

For the numerical solution to these equations to be stable (bounded with respect to time), the ratio $\Delta x/\Delta t$ must equal or exceed the maximum fluid plus sound speed encountered anywhere in the fluid. This criterion was derived originally from linearized equations, but has been found to be sufficient for the general nonlinear equations. In essence, this constraint on the grid dimensions requires that calculations proceed through the flowfield at a rate $(\Delta x/\Delta t)$ greater than or equal to the physical propagation rate $(u + a)$. If this condition were not satisfied, perturbations could only be transmitted through the flow at the nonphysical rate of $\Delta x/\Delta t$, resulting in gibberish. When this condition is satisfied, perturbations propagate through the field at the physical rate of $u \pm a$, and the only information transmitted at the rate $\Delta x/\Delta t$ is the truncation and roundoff errors. We therefore define u_r to be a maximum average value of local flow velocity and sound speed,

$$u_r = (\tfrac{1}{2})[|u| + a]_{\max} \tag{7}$$

Therefore,

$$(\Delta x/\Delta t)/2u_r \approx 1.0 \tag{8}$$

The ratio $x_r/\Delta x$ is simply the number of nodes in the spatial field at which calculations are made. Let

$$N = x_r/\Delta x \tag{9}$$

The normalized governing differential equations, after dropping the subscript o, are:

mass,

$$\partial(\rho A)/\partial t + \partial(\rho A u)/\partial x + \psi = (1/N)[\partial^2(\rho A)/\partial x^2]$$

momentum,

$$\partial(\rho A u)/\partial t + \partial(\rho A u^2)/\partial x + \psi u = -A(\partial P/\partial x) + (1/N)[\partial^2(\rho A u)/\partial x^2] \tag{10}$$

and energy,

$$(\partial/\partial t)\{(\rho A)[P/(\gamma - 1)\rho + u^2/2]\} + (\partial/\partial x) \times \{(\rho A u)[\gamma P/(\gamma - 1)\rho + u^2/2]\} + \psi[\gamma P/(\gamma - 1)\rho + u^2/2] = (1/N)(\partial^2/\partial x^2)\{(\rho A)[P/(\gamma - 1)\rho + u^2/2]\}$$

Therefore, the normalized governing differential equations are independent of model size and the additional second-order terms depend only on the number of nodes in the field. If, in addition, the initial and boundary conditions are similarly scaled, then geometrically similar flow systems are dynamically similar, and the solution of any one inlet problem yields the solutions to all equivalently scaled problems.

Numerical Compressor Face Boundary Conditions

The one-dimensional analog of an axisymmetric inlet is a simple converging-diverging nozzle with the left-hand boundary at the cowl lip and the right-hand boundary at the compressor face. For the started mixed-compression inlet simulation problems, the supersonic left-hand boundary conditions can be prescribed independently of the downstream flow. The subsonic right-hand boundary conditions, however, must account in some fashion for the dynamic interaction of the subsonic diffuser with the upstream supersonic flow and the downstream compressor.

Completely defining the numerical solution of the three conservation equations in this initial-boundary value problem requires that three boundary conditions be specified at the compressor face. Since the corrected weight flow parameter (compressor face Mach number and flow area) is conventionally used to describe engine operation, its temporal variation was selected as one boundary condition. Possible alternatives for the two remaining conditions include prescribing the flow variables or their derivatives or extrapolating their corresponding difference equations. In view of the myriad possibilities and the general scarcity of definitive supporting dynamic experimental data, two sets of additional boundary conditions were selected as being representative: 1) zero flow gradients at the boundary and 2) extrapolated difference equations.

A review of the available experimental data indicated that there was considerable latitude in choosing a representative compressor face Mach number history during surge. Therefore, as a test case, impulsively setting the Mach number equal to zero was selected as being an appropriate intermediate temporal flow variation which would also provide solutions that might be compared with the closed-form solutions obtained with the transformed Rankine-Hugoniot (R-H) equations. The over-all effects of using these different boundary conditions were then examined via the following problem. Given a constant area duct with an initially uniform $M = 2.0$ flow, the corrected weight flow at the right-hand boundary is set equal to zero, the weight flow at the left-hand boundary being held constant at $M = 2.0$. A shock wave is formed and begins moving to the left. At $t = 1.0 \times 10^{-3}$ sec, the right-hand boundary corrected weight flow is returned to its original value and held constant. An expansion wave is formed, moves to the left, overtakes and attenuates the shock wave, and the fluid compressed by the initial shock wave finally flows out of the field to the right.

Given that the corrected weight flow (Mach number) prescription replaces one of the three conservation equations, the two remaining flow properties are calculated from the assumed conditions. Assuming that the first backward spatial difference is consistent with or reasonably represents

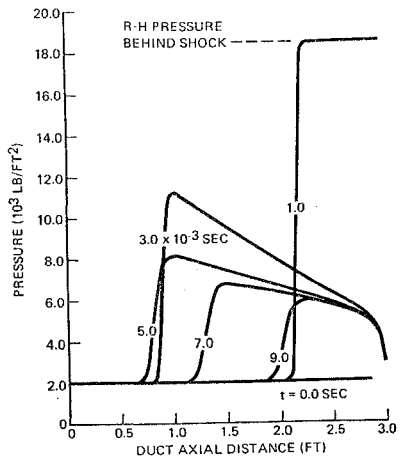

Fig. 3 Duct pressure history.

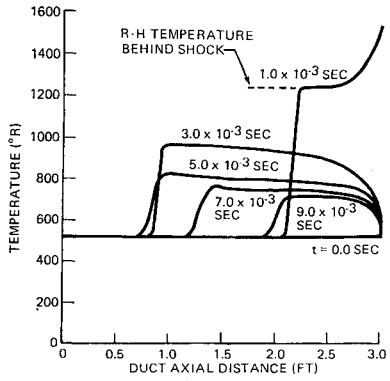

Fig. 4 Duct temperature history.

its differential equivalent, we can calculate boundary flow properties from

$$(\partial\rho/\partial x)_l^n = 0 \rightarrow \rho_l^n = \rho_{l-1}^n, \quad (\partial P/\partial x)_l^n = 0 \rightarrow P_l^n = P_{l-1}^n$$
$$u_l^n = M_l^n[(\gamma P/\rho)^{1/2}]_l^n, \quad M_l^n = 2.0(t = 0.0)$$
$$M_l^n = 0.0(0.0 < t \leq 1.0 \times 10^{-3}\ \text{sec})$$
$$M_l^n = 2.0(t > 1.0 \times 10^{-3}\ \text{sec}) \qquad (11)$$

where the subscript l indicates the right-hand boundary.

Similarly, using the first backward spatial difference and the first forward time difference, we can extrapolate the mass and energy equations, yielding,

$$(\rho A)_l^{n+1} = (\rho A)_l^n - (\Delta t/\Delta x)[(\rho Au)_l^n - (\rho Au)_{l-1}^n] - \Delta t\psi_l^n$$
$$\{(PA)[(2 + \gamma(\gamma - 1)M^2)/2(\gamma - 1)]\}_l^{n+1} = \{(PA)[(2 + \gamma(\gamma - 1)M^2)/2(\gamma - 1)]\}_l^n - \Delta t/\Delta x\{[\rho Au(\gamma P/\rho(\gamma - 1) + u^2/2)]_l^n - [\rho Au(\gamma P/\rho(\gamma - 1) + u^2/2)]_{l-1}^n\} - \Delta t\{\psi \times [\gamma P/\rho(\gamma - 1) + u^2/2]\}_l^n \qquad (12)$$
$$u_l^{n+1} = [M(\gamma P/\rho)^{1/2}]_l^{n+1}$$

Extensive numerical experimentation revealed that increasing the backward difference approximations to second third, or fourth order had little effect on the resulting boundary values, but that the order in which the flow variables were calculated could be interchanged for other relatively slow Mach number transients only. For example, extrapolating the momentum and energy equations and calculating ρ_l^{n+1} from the Mach number prescription produced large nonphysical excursions in pressure which, unless artificially bounded, ultimately produced negative pressures. For these other flow variable calculations, the boundary Mach number was not set identically equal to zero for $0 < t \leq 1.0 \times 10^{-3}$ sec, but equal to 1.0×10^{-6}. Artificially bounding the boundary conditions was avoided wherever possible since it introduced nonphysical constraints that only complicated the problem and the interpretation of the results.

Figure 3 shows the duct static pressure profiles at the indicated times for the zero gradients prescription. The pressure history obtained from the extrapolated equations prescription was identical to that shown in the figure. The pressure behind the initial shock obtained from the R-H equations is also shown. Figure 4 shows the temperature profile history for the extrapolated equations condition. While the temperatures away from the boundary were identical to the zero gradient and R-H values in the initial wave (the R-H equations also effectively presume zero flow gradients on either size of the initial wave), those adjacent to the right-hand boundary varied considerably. The boundary temperature behind the initial wave exceeded the R-H value by 310°R.

When the Mach number was again set equal to 2.0, both flows experienced large gradients adjacent to the boundary as a result of the very rapid reacceleration of the fluid required to satisfy this new boundary Mach number. Intuitively, one would expect to encounter such large boundary gradients in response to rapid boundary fluctuations in both the initial and subsequent waves, as observed in the extrapolated equations conditions, while the zero gradients prescription would be more representative of the flow variations resulting from less severe transients. Since the pressure history variation was the primary objective, the temperature sensitivity was not critical. However, it is interesting to note than even when the only explicit connection with the engine or downstream flow is the Mach number prescription and the pressure and density are actually calculated from the upstream flow properties, significant variations in the temperature flow history can occur.

Since the pressure history adjacent to the imagined compressor face was not significantly altered by the choice of the additional boundary conditions (zero gradients or extrapolated equations) in the preceding exercise, one then might ask: How sensitive is the maximum pressure rise in a duct following surge to the temporal engine corrected weight flow definition of the surge? Defining surge requires at least two quantities: the amplitude of the fluctuation in corrected weight flow and the time interval over which this fluctuation occurred. One should actually prescribe the exact flow history at the compressor face, but this is a most elusive quantity. Surge therefore was defined as a simple ramp reduction for this discussion. As before, the amplitude of surge was assumed to a 100% reduction; the time interval was varied from 1.0×10^{-6} sec (impulsive stoppage) to 5.0×10^{-2} sec. The inlet model was a converging diverging duct, similar to that shown in Fig. 1, with a contraction ratio of 2.0, an entering Mach number of 2.30, and a normal shock just downstream of the throat.

Figure 5 shows the peak pressure just upstream of the right-hand boundary following the 100% ramp reduction over the indicated time intervals. When the reduction was quite rapid, a second shock wave appeared at the compressor face whose strength (as defined by the static pressure ratio across the shock), increased as it propagated upstream in the subsonic diffuser. On reaching the throat, it coalesced with the standing normal shock and the newly formed shock moved into the supersonic diffuser. While the new shock continued to accelerate (increasing strength), the absolute pressure behind the shock began decreasing, producing expansion waves that propagated downstream, reduced the pressure in the subsonic diffuser, and locally reversed the flow. This sequence of events is depicted in Fig. 6, which shows the duct pressure profiles at the indicated elapsed time following the impulsive flow stoppage at the compressor face.

In Fig. 5, note that as the surge time interval is increased, the peak pressure decreases in the subsonic diffuser. This can be explained in terms of the conflicting effects of 1) the pressure rise resulting from the upstream travel of compression waves as the compressor flow is reduced and 2) the pressure drop resulting from the downstream travel of expansion waves as the original standing normal shock is nudged into the

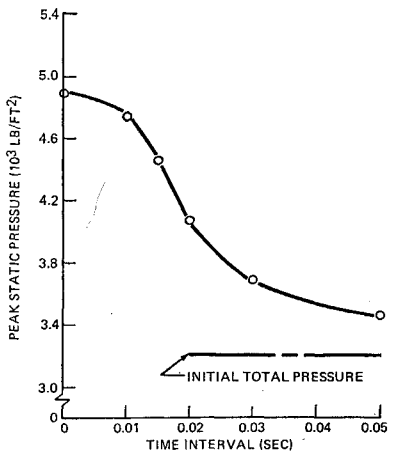

Fig. 5 Peak pressure following surge.

supersonic diffuser by the upstream-traveling compression waves. The resulting pressure rise is determined by the dominance of one of these events. For very rapid flow reductions, the upstream travel of compression waves dominates, while for slow transients, the standing normal shock expulsion is the controlling factor. Between the two extremes, the pressure rise is sensitive to the flow reduction rate.

Inlet Geometry and Auxiliary Air Systems

Inlet pressure history during surge is quite sensitive to inlet geometry. Using the impulsive flow stoppage model of surge, the peak pressure is a strong function of the inlet contraction ratio (the ratio of compressor face to throat flow areas) and the initial compressor face Mach number. The inlet volume had little effect on the peak pressure, but it did influence the duration of the pressure pulse. However, future studies in which the engine is more realistically coupled to the inlet will undoubtedly attach increased importance to the inlet volume and how it influences the recovery characteristics of the engine following surge. Figure 7 shows the peak compressor face static pressure ratio reached for four different contraction ratio ducts following surge as a function of initial compressor face Mach number. The maximum pressure was independent of whether the upstream boundary was supersonic or subsonic. However, for the supersonic upstream flow cases, when the terminal normal shock was located considerably downstream of the throat in the subsonic diffuser, the peak pressures departed from the indicated curves, the peak pressures being lower than those shown. In the preliminary design of inlets, such changes must be taken into account. For example, increasing the design thrust of a prospective propulsion system by overspeeding the engine, thereby increasing the design compressor face Mach number, may ultimately result in a net loss of additional thrust because of the increased weight of the inlet necessary to withstand the higher peak surge pressure.

Each auxiliary air system tends to reduce the inlet peak pressure during surge. Figure 8 shows compressor face pressure histories for a typical inlet configuration with and without throat slot and secondary air systems. The boundary-layer bleed was the same in both cases and the bypass doors were closed. The initial increase in pressure following the impulsive flow stoppage is simply a function of the initial compressor face Mach number. This is reflected in the small difference in the initial rise resulting from the small difference in initial compressor face Mach numbers for the two cases. As the compression or shock wave is formed and begins moving upstream toward the throat, the bleeding capacity of the secondary air system becomes apparent. The difference in the compressor face static pressures increases with increasing time. The throat slot becomes effective once the surge normal shock coalesces with the standing normal shock and the the shock moves into the throat region. When the shock wave passes the throat and moves into the converging portion of the duct, expansion waves begin propagating into the subsonic diffuser, which, depending on the initial Mach number distribution and inlet contraction ratio, may locally reverse the flow. Of course, once the shock wave has propagated upstream of the cowl lip, the higher internal duct pressure will locally reverse the flow until the internal pressure drops below the external total pressure. It was assumed that no coupling existed between the main duct flow and the auxiliary systems. Once the engine surged, the main duct pressure increased rapidly, thereby choking the auxiliary duct's entrances. The volume of these ducts was sufficiently large and the surge duration sufficiently short to prevent the back pressures from increasing to the point where the duct's entrance nozzles unchoked. Additional dynamic studies of the secondary air system ducts, for example, have shown that because of its relatively small entrance nozzle area and large volume, the average duct pressure does not increase appreciably during surge.

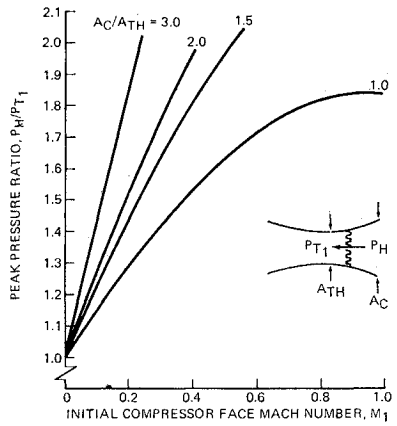

Fig. 7 Contraction ratio effect.

Experimental Evidence

Alford and Victor[8] examined the stall characteristics of a large turbojet engine in response to the impulsive addition of a slug of fuel to the combustion chamber. Pressures and temperatures were recorded in the bell-mouthed constant area duct mounted ahead of the engine. A long bullet nose, extending nearly one-third of the 120-in. duct length, was attached to the compressor face. Figure 9 shows the temperature history just upstream of the compressor face after the addition of the slug of fuel. The first pronounced temperature rise is due to the compressive heating of the gas by the compression wave propagating upstream. The second, and far larger, temperature peak is due to the local flow reversal where the burned gas is now flowing upstream. At this point the fuel pulse has been expended, the compressor has recovered from the stall and begun passing large amounts of air again, and the temperature has dropped to its original level. The flow reversal was not circumferentially or radially uniform, and the upstream travel and strength of the temperature wave was attenuated by mixing with the unreversed cool gas flow. Figure 10 is the pressure history just upstream of the compressor for a similar stall. Plane I was located 79.5-in. upstream of the compressor face and plane III was

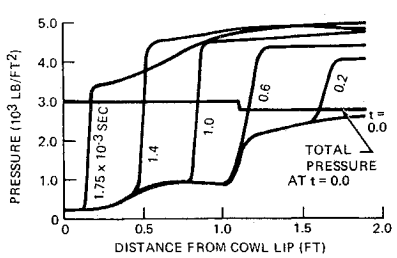

Fig. 6 Inlet pressure history.

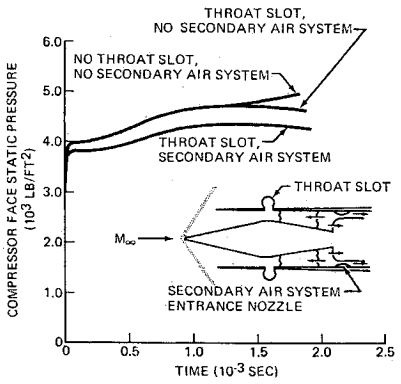

Fig. 8 Auxiliary air system effect.

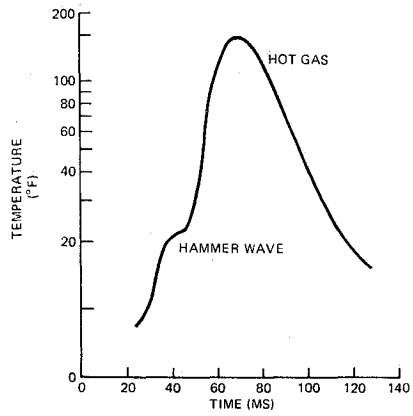

Fig. 9 Inlet temperature rise following stall at plane I (Ref. 8).

5.75-in. upstream. The ratio of peak to initial static pressure is 1.32. The second smaller pressure peak is a reflection of the first wave from the upstream end of the duct.

The authors maintain that similar tests conducted with simulated hard afterburner lightoffs produced similar, although smaller, inlet pressure and temperature excursions. Their conclusions were that compressor surges induced by this fuel addition method would produce large temperature and pressure variations, but that simulating the type of surge by a complete and instantaneous flow stoppage was inaccurate, since it underestimated the temperature variations (no consideration was given to the reverse flow of burned gas) and overestimated the pressure changes (the radial and circumferential nonuniformity of the flow allowed the simultaneous upstream travel of the burned gases and the downstream travel of the unburned fluid). As discussed in their Appendix C, at the measured duct Mach number of 0.37 the peak to initial static pressure ratio would be approximately 1.65 if the flow were completely and instantaneously stopped.

Rowe[9] investigated the surge characteristics of a two-stage compressor (one axial, one centrifugal) by throttling the compressor's exhaust valve and measuring pressures and temperatures in the constant area annular duct 5.75 ft in length mounted ahead of the compressor. The compressor was driven by a separate turbine. The experimental apparatus is illustrated in Fig. 11. The duct flow history following surge at 100% design speed is shown in Fig. 12. The curves displaced to the right are numerical results and are discussed in the following section. The total pressure and temperature probes and the static pressure P_1 were located 0.50-ft upstream of the compressor face. The static pressures P_3 and P_5 were located 2.50 ft and 4.50 ft, respectively, upstream of the compressor face. Prior to surge, the upstream-facing total pressure and total temperature probes observe the stream total pressure and temperature, whereas the other probes, being partially shielded by the probes themselves and facing downstream, observe somewhat lower values.

After the onset of surge, the initial upstream-traveling compression wave locally reverses the flow, causing P_{TR} now facing the oncoming flow, to be higher than P_{TF}. Once the initial compression wave reaches the upstream boundary, it is reflected as an expansion wave, thereby increasing the flow in the reverse direction and decreasing the duct pressure. The pressure rise following the initial drop occurs because of 1) the high-pressure air flowing backwards out of the compressor and because 2) the compressor, once surged, acts much like a solid boundary, reflecting incident compression waves as compression waves and expansion waves as expansion waves. This causes the pressure to again rise after the initial compression wave has been twice reflected from the duct entrance boundary. The "W" shape of this second smaller pressure peak, as stated by Rowe, "is probably caused by reflection from the walls of the test cell," located a short distance ahead of the duct entrance. P_1 peak to initial static pressure ratios as high as 2.42 were recorded following surge at the 100% design speed. P_5, being nearest to the duct entrance, recorded the lowest static pressure rise.

During surge, the measured total temperature peaks, corrected for the thermocouples thermal lag, considerably exceeded those calculated from the measured pressure rises and the transformed Rankine-Hugoniot equations. This difference was attributed to the large circumferential flow velocity imparted to the fluid flowing backwards (upstream) through the compressor during the period of reversed flow. This circumferential kinetic energy measured by the thermocouples would not be observed by the axially mounted total pressure probes.

Following the initial large flow pulsations, the duct pressure was gradually reduced to the ambient external pressure as the high-pressure duct air was exhausted out of the duct entrance and the high-pressure air in the plenum chamber downstream of the compressor was exhausted through the partially open throttling valve. The compressor then recovered from surge, sending an expansion wave through the duct which momentarily lowered the duct static pressure below its initial steady-state value, and restablished flow in the forward direction. Once the surge had been initiated by slightly closing the downstream throttling valve, the complete flow oscillation cycle, as depicted in Fig. 12, recurred at a frequency of about 3.50 Hz until the valve was reopened. The frequency of oscillation increased and the amplitudes of the flow pulsations decreased at the lower wheel speeds.

Additional unpublished experimental data were obtained when a modified JT8D-1 engine with a 727 center engine S-shaped inlet duct surged unexpectedly during routine performance tests. The duct was then instrumented to record the maximum static pressures encountered during surge. The peak static to initial total pressure ratios measured varied from approximately 1.41 to 1.49. The peak to initial static pressure ratio ranged from approximately 1.60 to 1.77. If one assumes that complete and instantaneous flow stoppage is the correct surge model, the calculated pressure rise exceeds the measured peak by 9%. The source of the engine surge was finally determined to be improperly positioned turbine second-stage nozzle guide vanes.

The combination of additional boundary conditions and corrected weight flow variations that is truly representative

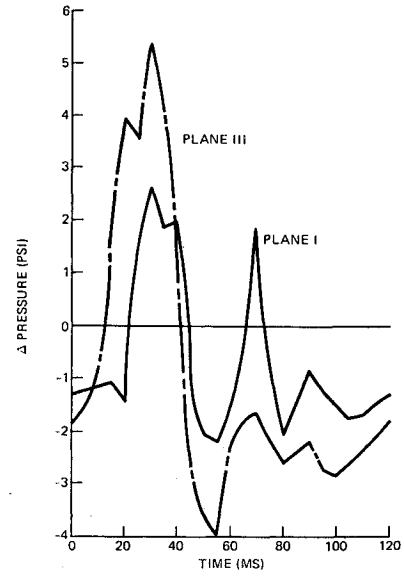

Fig. 10 Static pressure variation in inlet following stall (Ref. 8).

of the supersonic transport propulsion system is the subject of much discussion and conjecture. The widely divergent results of the tests discussed, although not all inclusive, indicate the sensitivity of the inlet flow following surge to the surge-initiating mechanism. In each case the duct overpressure exceeded the initial stream total pressure. In the high-altitude, high Mach number environment of a supersonic transport, such overpressures result in very large pressure differentials across the inlet structure. Extensive studies have been conducted within the Boeing Company to determine the peak overpressure resulting from the most severe combination of Mach number, altitude, and engine transients. However, the interaction of the various components of this system will undoubtedly require that several different sets of boundary conditions be used to define surge. The moot questions surrounding this problem must be deferred until the extensive dynamic testing of the entire propulsion system is completed.

Comparison of Numerical Model with Experimental Data

Any quantitative comparison of numerical results with experimental data is complicated by 1) our inability to define the exact surge and recovery characteristics of a given compressor as outlined previously and 2) the interaction of the compressor-generated transients with the upstream duct entrance boundary. The initial pressure rise, as experimentally measured at some upstream duct position, can be reproduced numerically by adjusting the initial compressor face corrected weight flow variation to yield the same pressure rise. However, any flow description beyond this point must account for the simultaneous recovery or continuing surge of the compressor and the downstream-traveling compression or expansion waves resulting from the interaction of the initial upstream-traveling compression waves with the upstream boundary.

The upstream boundary conditions depend on both duct entrance geometry and external flow environment. Rudinger[4] and Foa[5] discuss these problems in some detail. The external flow may be supersonic or subsonic and traveling in the same or opposite direction as the initial flow in the duct, or the flow may be quiescent. If the length/diameter of the duct is large and the flow perturbations are small, the erratic flow following a wave reflection at the duct entrance plane will be attenuated before it can appreciably affect the flow some distance downstream. The calculated flow history, using pseudo-steady boundary conditions (such as constant entrance plane static pressure), some distance downstream then would differ only slightly from that observed experimentally. Airplane inlets, however, are typically short and squatty with length/diameter ratios of about 3. Because of this highly three-dimensional boundary interaction, it is difficult to obtain quantitative agreement between experimental and numerical data, especially when the initial waves are strong enough to produce backflow from the duct entrance and markedly change the external flow.

In view of the exploratory nature of this investigation and the availability of Rowe's detailed dynamic data, the quiescent external environment boundary condition was selected for evaluation. The effective length/diameter ratio of the annular duct was about 15.5. Numerical experiments were conducted using the impulsive flow stoppage model of surge in a constant area duct (similar to that used for the right-hand boundary studies) as a test case. This study showed that the most physically realistic conditions resulted from assuming zero second spatial derivatives for each of the variables, ρ, u, and P at the boundary, subject to the constraint that the duct total pressure always was greater than or equal to the assumed external ambient pressure. This additional restriction prevented the duct total pressure from dropping below the assumed external ambient pressure before the compressor could recover from surge and restablish the steady flow existing in the duct prior to surge.

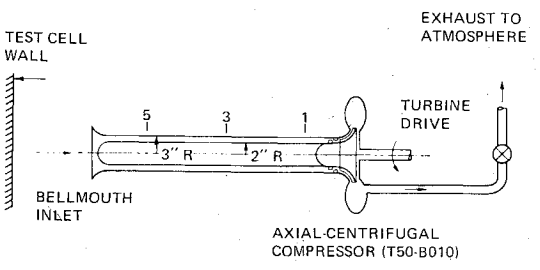

Fig. 11 Experimental apparatus.

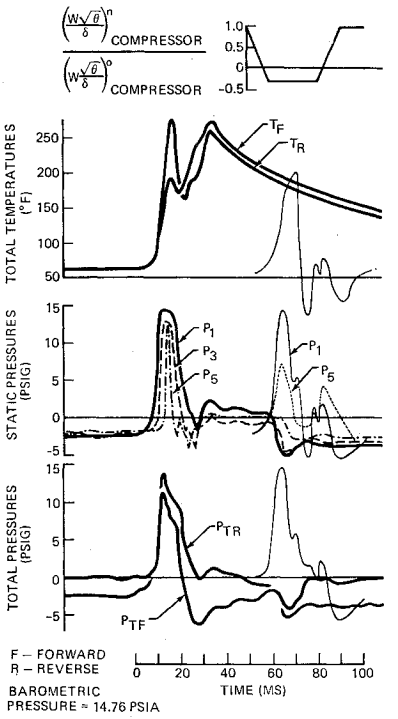

Fig. 12 Duct flow history (Ref. 9).

The corrected weight flow variation at the right-hand boundary simulating the surge and recovery characteristics of the compressor was estimated from the experimentally observed static pressure history at station 1. The zero gradients prescription discussed earlier was used for the additional compressor face boundary conditions. Numerical results are shown in Fig. 12 (displaced to the right by 50 ms for clarity). Even using the simple corrected weight flow variation indicated in the figure, the numerical model can approximately reproduce the duct flow history following surge. The calculated total pressure and temperature should be interpreted as the greater of the two measured values of each variable since the calculated values do not take into account the flow direction relative to the probes. Although the calculated total pressure history agrees well with the measured value, the calculated total temperature peak is somewhat lower than the corresponding measured peak. This results from the large circumferential flow velocities, which are, of course, not considered in this one-dimensional model. The blip appearing on the right-hand side of the initial pressure spikes at station 1 was caused by the overly simplistic left-hand boundary conditions adjusting to the reverse flow of high-pressure fluid out of the duct entrance. This erratic adjustment is more apparent in P_5 adjacent to the duct entrance. This blip carries through the duct flow and appears as a slight drop in pressure and temperature in the second smaller spikes. Considering the relative simplicity of the boundary conditions used (both

left and right), it is apparent that a more detailed numerical investigation of a given propulsion system would yield a fairly accurate description of the inlet dynamics in response to prescribed freestream or engine transients. Representing observable and explainable physical phenomena by these artificial numerical methods and obtaining seemingly fortuitous agreement may appear disconcerting at first. But unless one is prepared to describe the exact temporal variation of each boundary flow variable during every flow transient, which is impossible, such agreement, fortuitous or not, is reassuring. As an illustration, had the extrapolated equations' boundary conditions been used instead of the zero gradients conditions in our comparison, the overly high temperatures near the compressor face (due physically to the circumferential velocities) could have been approximated numerically. (Recall that the boundary temperature considerably exceeded the Rankine-Hugoniot value on the right-hand boundary numerical experiment). Well-reasoned hypotheses could be devised that purport to explain the behavior of these numerical approximations, but these arguments border on the metaphysical. Faced with innumerable alternative methods of numerically prescribing boundary conditions, the pragmatist must select, however arbitrarily, some combination of boundary conditions that seems intuitively reasonable, then conduct his own numerical experiments.

Conclusions

The inherent simplicity and flexibility of the artificial viscosity technique make it well suited to solving general duct dynamics problems. However, the inclusion of nonphysical dissipative terms may preclude using this type of analysis on problems involving small-amplitude (acoustic) phenomena because of the relatively large number of nodes required to suppress these nonphysical terms. The wave thickness, and therefore the resolution of the flow transients, varies inversely with the number of nodes in the spatial field (N) and the wave strength. Therefore, in order to delineate relatively weak wave interactions, there must be a corresponding increase in the number of spatial nodes to compensate for the increased wave thickness of the weaker waves. As an example, when the CDC 6600 computer is used, the ratio of machine to real time is about 6000 for the problems described here, N being about 200. The higher flow resolution required for small-amplitude problems would at least quadruple this ratio.

Using the engine corrected weight flow parameter to describe dynamic engine behavior is satisfactory, providing that its temporal variation and the two remaining boundary conditions are judiciously selected to represent the particular propulsion system under consideration. The sensitivity of the inlet flow history to the surge-initiating mechanism requires that several such alternative boundary conditions be investigated. The peak pressure experienced by the inlet during compressor surge is very sensitive to the inlet contraction ratio and to the presence of auxiliary air systems.

References

[1] Wasserbauer, J. F. and Willoh, R. G., "Experimental and Analytical Investigation of the Dynamic Response of a Supersonic Mixed-Compression Inlet," TM X-52441, 1968, NASA.

[2] Chun, K. S. and Swanson, D. B., "Dynamic Simulation of Supersonic Inlet and Engine," AIAA Paper 64-598, Seattle, Wash., Aug. 1964.

[3] Martin, A. W., "Propulsion System Dynamic Simulation Theory and Equations," CR-73115, April 1967, NASA.

[4] Rudinger, G., *Wave Diagrams for Nonsteady Flow in Ducts*, Van Nostrand, New York, 1950.

[5] Foa, J. V., *Elements of Flight Propulsion*, Wiley, New York, 1960.

[6] Stroud, J. F., et al., "Inlet-Exhaust-Thrust Reverser Program for the Commercial Supersonic Transport," Lockheed Final Report, 16261-3, July 1963, Burbank, Calif.

[7] Lax, P. D., "Weak Solutions of Nonlinear Hyperbolic Equations and Their Numerical Computation," *Communications of Pure Applied Mechanics*, Vol. 7, No. 1, 1954, pp. 159–193.

[8] Alford, J. S. and Victor, I. W., "Dynamic Measurements of Forward Gas Expulsion During High Speed Stall of Jet Engines," *SAE Journal*, Vol. 75, No. 3, 1967.

[9] Rowe, M., "The Effect of Compressor Surge on the Flow in an Annular Duct Upstream of an Axial-Centrifugal Compressor," D6-20377, 1968, Boeing Co., Seattle, Wash.